Search for Scalar Top and Scalar Bottom Quarks at $\sqrt{s} = 189$ GeV at LEP

The OPAL Collaboration

Abstract

Searches for a scalar top quark and a scalar bottom quark have been performed using a data sample of 182 pb^{-1} at a centre-of-mass energy of $\sqrt{s}$ =189 GeV collected with the OPAL detector at LEP. No evidence for a signal was found. The 95% confidence level (C.L.) lower limit on the scalar top quark mass is 90.3 GeV if the mixing angle between the supersymmetric partners of the left- and right-handed states of the top quark is zero. In the worst case, when the scalar top quark decouples from the Z^0 boson, the lower limit is 87.2 GeV. These limits were obtained assuming that the scalar top quark decays into a charm quark and the lightest neutralino, and that the mass difference between the scalar top quark and the lightest neutralino is larger than 10 GeV. The complementary decay mode of the scalar top quark decaying into a bottom quark, a charged lepton and a scalar neutrino has also been studied. From a search for the scalar bottom quark, a mass limit of 88.6 GeV was obtained if the mass difference between the scalar bottom quark and the lightest neutralino is larger than 7 GeV. These limits significantly improve the previous OPAL limits.

The OPAL Collaboration

G. Abbiendi[2], K. Ackerstaff[8], G. Alexander[23], J. Allison[16], N. Altekamp[5], K.J. Anderson[9],
S. Anderson[12], S. Arcelli[17], S. Asai[24], S.F. Ashby[1], D. Axen[29], G. Azuelos[18,a], A.H. Ball[17],
E. Barberio[8], R.J. Barlow[16], J.R. Batley[5], S. Baumann[3], J. Bechtluft[14], T. Behnke[27],
K.W. Bell[20], G. Bella[23], A. Bellerive[9], S. Bentvelsen[8], S. Bethke[14], S. Betts[15], O. Biebel[14],
A. Biguzzi[5], V. Blobel[27], I.J. Bloodworth[1], P. Bock[11], J. Böhme[14], D. Bonacorsi[2],
M. Boutemeur[34], S. Braibant[8], P. Bright-Thomas[1], L. Brigliadori[2], R.M. Brown[20],
H.J. Burckhart[8], P. Capiluppi[2], R.K. Carnegie[6], A.A. Carter[13], J.R. Carter[5], C.Y. Chang[17],
D.G. Charlton[1,b], D. Chrisman[4], C. Ciocca[2], P.E.L. Clarke[15], E. Clay[15], I. Cohen[23],
J.E. Conboy[15], O.C. Cooke[8], C. Couyoumtzelis[13], R.L. Coxe[9], M. Cuffiani[2], S. Dado[22],
G.M. Dallavalle[2], R. Davis[30], S. De Jong[12], A. de Roeck[8], P. Dervan[15], K. Desch[8], B. Dienes[33,d],
M.S. Dixit[7], J. Dubbert[34], E. Duchovni[26], G. Duckeck[34], I.P. Duerdoth[16], P.G. Estabrooks[6],
E. Etzion[23], F. Fabbri[2], A. Fanfani[2], M. Fanti[2], A.A. Faust[30], F. Fiedler[27], M. Fierro[2], I. Fleck[10],
R. Folman[26], A. Frey[8], A. Fürtjes[8], D.I. Futyan[16], P. Gagnon[7], J.W. Gary[4], J. Gascon[18],
S.M. Gascon-Shotkin[17], G. Gaycken[27], C. Geich-Gimbel[3], G. Giacomelli[2], P. Giacomelli[2],
V. Gibson[5], W.R. Gibson[13], D.M. Gingrich[30,a], D. Glenzinski[9], J. Goldberg[22], W. Gorn[4],
C. Grandi[2], K. Graham[28], E. Gross[26], J. Grunhaus[23], M. Gruwé[27], G.G. Hanson[12],
M. Hansroul[8], M. Hapke[13], K. Harder[27], A. Harel[22], C.K. Hargrove[7], M. Hauschild[8],
C.M. Hawkes[1], R. Hawkings[27], R.J. Hemingway[6], M. Herndon[17], G. Herten[10], R.D. Heuer[27],
M.D. Hildreth[8], J.C. Hill[5], P.R. Hobson[25], M. Hoch[18], A. Hocker[9], K. Hoffman[8], R.J. Homer[1],
A.K. Honma[28,a], D. Horváth[32,c], K.R. Hossain[30], R. Howard[29], P. Hüntemeyer[27],
P. Igo-Kemenes[11], D.C. Imrie[25], K. Ishii[24], F.R. Jacob[20], A. Jawahery[17], H. Jeremie[18],
M. Jimack[1], C.R. Jones[5], P. Jovanovic[1], T.R. Junk[6], J. Kanzaki[24], D. Karlen[6],
V. Kartvelishvili[16], K. Kawagoe[24], T. Kawamoto[24], P.I. Kayal[30], R.K. Keeler[28], R.G. Kellogg[17],
B.W. Kennedy[20], D.H. Kim[19], A. Klier[26], T. Kobayashi[24], M. Kobel[3,e], T.P. Kokott[3],
M. Kolrep[10], S. Komamiya[24], R.V. Kowalewski[28], T. Kress[4], P. Krieger[6], J. von Krogh[11],
T. Kuhl[3], P. Kyberd[13], G.D. Lafferty[16], H. Landsman[22], D. Lanske[14], J. Lauber[15],
S.R. Lautenschlager[31], I. Lawson[28], J.G. Layter[4], A.M. Lee[31], D. Lellouch[26], J. Letts[12],
L. Levinson[26], R. Liebisch[11], B. List[8], C. Littlewood[5], A.W. Lloyd[1], S.L. Lloyd[13],
F.K. Loebinger[16], G.D. Long[28], M.J. Losty[7], J. Lu[29], J. Ludwig[10], D. Liu[12], A. Macchiolo[2],
A. Macpherson[30], W. Mader[3], M. Mannelli[8], S. Marcellini[2], C. Markopoulos[13], A.J. Martin[13],
J.P. Martin[18], G. Martinez[17], T. Mashimo[24], P. Mättig[26], W.J. McDonald[30], J. McKenna[29],
E.A. Mckigney[15], T.J. McMahon[1], R.A. McPherson[28], F. Meijers[8], S. Menke[3], F.S. Merritt[9],
H. Mes[7], J. Meyer[27], A. Michelini[2], S. Mihara[24], G. Mikenberg[26], D.J. Miller[15], R. Mir[26],
W. Mohr[10], A. Montanari[2], T. Mori[24], K. Nagai[8], I. Nakamura[24], H.A. Neal[12], R. Nisius[8],
S.W. O'Neale[1], F.G. Oakham[7], F. Odorici[2], H.O. Ogren[12], M.J. Oreglia[9], S. Orito[24],
J. Pálinkás[33,d], G. Pásztor[32], J.R. Pater[16], G.N. Patrick[20], J. Patt[10], R. Perez-Ochoa[8],
S. Petzold[27], P. Pfeifenschneider[14], J.E. Pilcher[9], J. Pinfold[30], D.E. Plane[8], P. Poffenberger[28],
B. Poli[2], J. Polok[8], M. Przybycień[8,f], C. Rembser[8], H. Rick[8], S. Robertson[28], S.A. Robins[22],
N. Rodning[30], J.M. Roney[28], S. Rosati[3], K. Roscoe[16], A.M. Rossi[2], Y. Rozen[22], K. Runge[10],
O. Runolfsson[8], D.R. Rust[12], K. Sachs[10], T. Saeki[24], O. Sahr[34], W.M. Sang[25],
E.K.G. Sarkisyan[23], C. Sbarra[29], A.D. Schaile[34], O. Schaile[34], P. Scharff-Hansen[8], J. Schieck[11],
S. Schmitt[11], A. Schöning[8], M. Schröder[8], M. Schumacher[3], C. Schwick[8], W.G. Scott[20],
R. Seuster[14], T.G. Shears[8], B.C. Shen[4], C.H. Shepherd-Themistocleous[8], P. Sherwood[15],
G.P. Siroli[2], A. Sittler[27], A. Skuja[17], A.M. Smith[8], G.A. Snow[17], R. Sobie[28],
S. Söldner-Rembold[10], S. Spagnolo[20], M. Sproston[20], A. Stahl[3], K. Stephens[16], J. Steuerer[27],

1

K. Stoll[10], D. Strom[19], R. Ströhmer[34], B. Surrow[8], S.D. Talbot[1], P. Taras[18], S. Tarem[22],
R. Teuscher[8], M. Thiergen[10], J. Thomas[15], M.A. Thomson[8], E. Torrence[8], S. Towers[6],
I. Trigger[18], Z. Trócsányi[33], E. Tsur[23], A.S. Turcot[9], M.F. Turner-Watson[1], I. Ueda[24],
R. Van Kooten[12], P. Vannerem[10], M. Verzocchi[10], H. Voss[3], F. Wäckerle[10], A. Wagner[27],
C.P. Ward[5], D.R. Ward[5], P.M. Watkins[1], A.T. Watson[1], N.K. Watson[1], P.S. Wells[8],
N. Wermes[3], J.S. White[6], G.W. Wilson[16], J.A. Wilson[1], T.R. Wyatt[16], S. Yamashita[24],
G. Yekutieli[26], V. Zacek[18], D. Zer-Zion[8]

[1]School of Physics and Astronomy, University of Birmingham, Birmingham B15 2TT, UK
[2]Dipartimento di Fisica dell' Università di Bologna and INFN, I-40126 Bologna, Italy
[3]Physikalisches Institut, Universität Bonn, D-53115 Bonn, Germany
[4]Department of Physics, University of California, Riverside CA 92521, USA
[5]Cavendish Laboratory, Cambridge CB3 0HE, UK
[6]Ottawa-Carleton Institute for Physics, Department of Physics, Carleton University, Ottawa, Ontario K1S 5B6, Canada
[7]Centre for Research in Particle Physics, Carleton University, Ottawa, Ontario K1S 5B6, Canada
[8]CERN, European Organisation for Particle Physics, CH-1211 Geneva 23, Switzerland
[9]Enrico Fermi Institute and Department of Physics, University of Chicago, Chicago IL 60637, USA
[10]Fakultät für Physik, Albert Ludwigs Universität, D-79104 Freiburg, Germany
[11]Physikalisches Institut, Universität Heidelberg, D-69120 Heidelberg, Germany
[12]Indiana University, Department of Physics, Swain Hall West 117, Bloomington IN 47405, USA
[13]Queen Mary and Westfield College, University of London, London E1 4NS, UK
[14]Technische Hochschule Aachen, III Physikalisches Institut, Sommerfeldstrasse 26-28, D-52056 Aachen, Germany
[15]University College London, London WC1E 6BT, UK
[16]Department of Physics, Schuster Laboratory, The University, Manchester M13 9PL, UK
[17]Department of Physics, University of Maryland, College Park, MD 20742, USA
[18]Laboratoire de Physique Nucléaire, Université de Montréal, Montréal, Quebec H3C 3J7, Canada
[19]University of Oregon, Department of Physics, Eugene OR 97403, USA
[20]CLRC Rutherford Appleton Laboratory, Chilton, Didcot, Oxfordshire OX11 0QX, UK
[22]Department of Physics, Technion-Israel Institute of Technology, Haifa 32000, Israel
[23]Department of Physics and Astronomy, Tel Aviv University, Tel Aviv 69978, Israel
[24]International Centre for Elementary Particle Physics and Department of Physics, University of Tokyo, Tokyo 113-0033, and Kobe University, Kobe 657-8501, Japan
[25]Institute of Physical and Environmental Sciences, Brunel University, Uxbridge, Middlesex UB8 3PH, UK
[26]Particle Physics Department, Weizmann Institute of Science, Rehovot 76100, Israel
[27]Universität Hamburg/DESY, II Institut für Experimental Physik, Notkestrasse 85, D-22607 Hamburg, Germany
[28]University of Victoria, Department of Physics, P O Box 3055, Victoria BC V8W 3P6, Canada
[29]University of British Columbia, Department of Physics, Vancouver BC V6T 1Z1, Canada
[30]University of Alberta, Department of Physics, Edmonton AB T6G 2J1, Canada

[31]Duke University, Dept of Physics, Durham, NC 27708-0305, USA
[32]Research Institute for Particle and Nuclear Physics, H-1525 Budapest, P O Box 49, Hungary
[33]Institute of Nuclear Research, H-4001 Debrecen, P O Box 51, Hungary
[34]Ludwigs-Maximilians-Universität München, Sektion Physik, Am Coulombwall 1, D-85748 Garching, Germany

[a] and at TRIUMF, Vancouver, Canada V6T 2A3
[b] and Royal Society University Research Fellow
[c] and Institute of Nuclear Research, Debrecen, Hungary
[d] and Department of Experimental Physics, Lajos Kossuth University, Debrecen, Hungary
[e] on leave of absence from the University of Freiburg
[f] and University of Mining and Metallurgy, Cracow

1 Introduction

Supersymmetric (SUSY) extensions of the Standard Model predict the existence of bosonic partners of all known fermions. The scalar top quark ($\tilde{t}$), which is the bosonic partner of the top quark, may be light because of supersymmetric radiative corrections [1]. Furthermore, the supersymmetric partners of the right-handed and left-handed top quarks ($\tilde{t}_R$ and $\tilde{t}_L$) mix, and the resultant two mass eigenstates ($\tilde{t}_1$ and $\tilde{t}_2$) have a mass splitting, which may be very large due to the large top quark mass. Then the lighter mass eigenstate ($\tilde{t}_1$), $\tilde{t}_1 = \tilde{t}_L \cos\theta_{\tilde{t}} + \tilde{t}_R \sin\theta_{\tilde{t}}$, where $\theta_{\tilde{t}}$ is a mixing angle, can be lighter than any other charged SUSY particle, and also lighter than the top quark [1]. All SUSY breaking parameters are hidden in the $\theta_{\tilde{t}}$ and the mass of $\tilde{t}_1$.

The scalar bottom quark ($\tilde{b}$) can also be light if $\tan\beta$, the ratio of vacuum expectation values of the two Higgs doublet fields, is larger than approximately 40. In this case, the analogous mixing between the supersymmetric partners of the right- and left-handed states of the bottom quark ($\tilde{b}_R$ and $\tilde{b}_L$) becomes large, and the resultant two mass eigenstates ($\tilde{b}_1$ and $\tilde{b}_2$) also have a large mass splitting [2]. The mass of the lighter mass eigenstate ($\tilde{b}_1$) may therefore be within the reach of LEP2.

Assuming R-parity [3] conservation, the dominant decay mode of the $\tilde{t}_1$ is expected to be either $\tilde{t}_1 \to c\tilde{\chi}_1^0$ or $\tilde{t}_1 \to b\tilde{\nu}\ell^+$, where $\tilde{\chi}_1^0$ is the lightest neutralino and $\tilde{\nu}$ is the scalar neutrino. The latter decay mode is dominant, if it is kinematically allowed. Otherwise the flavour changing two-body decay, $\tilde{t}_1 \to c\tilde{\chi}_1^0$, is dominant except for the small region of $m_{\tilde{t}_1} - m_{\tilde{\chi}_1^0} > m_{W^\pm} + m_b$[1]. Both of these decay modes ($\tilde{t}_1 \to c\tilde{\chi}_1^0$ and $\tilde{t}_1 \to b\tilde{\nu}\ell^+$) have been searched for. The dominant decay mode of the $\tilde{b}_1$ is expected to be $\tilde{b}_1 \to b\tilde{\chi}_1^0$. Under the assumption of R-parity conservation, $\tilde{\chi}_1^0$ and $\tilde{\nu}$ are invisible in the detector. Thus, $\tilde{t}_1\bar{\tilde{t}}_1$ and $\tilde{b}_1\bar{\tilde{b}}_1$ events are characterised by two acoplanar jets[2] or two acoplanar jets plus two leptons, with missing energy. The phenomenology of the production and decay of $\tilde{t}_1$ ($\tilde{b}_1$) is described in Section 2 of Ref. [4].

---

[1]In this region, $\tilde{t}_1 \to b\tilde{\chi}_1^0 W^+$(on shell) becomes dominant through a virtual chargino as described in Section 4. This decay mode has not been searched for in this paper.

[2]Two jets are called 'acoplanar' if they not back-to-back with each other in the plane perpendicular to the beam axis.

The D0 Collaboration has reported a lower limit [5] on the $\tilde{t}_1$ mass of about 85 GeV (95% C.L.) for the case that $\tilde{t}_1 \to c\tilde{\chi}_1^0$ is the dominant decay mode and the mass difference between $\tilde{t}_1$ and $\tilde{\chi}_1^0$ is larger than about 35 GeV. Searches at e^+e^- colliders are sensitive to a smaller mass difference. Mass limits for the $\tilde{t}_1$ have already been obtained around the Z^0 peak (LEP1) assuming $\tilde{t}_1 \to c\tilde{\chi}_1^0$ [6]. A 95% C.L. lower limit of 76 GeV for a mass difference larger than 5 GeV has been obtained as a result of previous searches at centre-of-mass energies 161 [7], 171 [4, 8] and 183 GeV [9, 10].

In 1998 the LEP e^+e^- collider at CERN was operated at $\sqrt{s}$ = 188.6 GeV, and a data sample of 182.1 pb^{-1} was collected with the OPAL detector. In this paper direct searches for $\tilde{t}_1$ and $\tilde{b}_1$ using this data sample are reported. The results shown here have been obtained by combining the results obtained at this new centre-of-mass energy with those previously obtained by the OPAL detector at $\sqrt{s}$ = 161, 171 and 183 GeV [7, 4, 9].

2 The OPAL Detector and Event Simulation

The OPAL detector, which is described in detail in Ref. [11], is a multipurpose apparatus having nearly complete solid angle coverage. The central detector consists of a silicon strip detector and tracking chambers, providing charged particle tracking for over 96% of the full solid angle, inside a uniform solenoidal magnetic field of 0.435 T. A lead-glass electromagnetic calorimeter (EM) located outside the magnet coil is hermetic in the polar angle[3] range of $|\cos\theta| < 0.82$ for the barrel region and $0.81 < |\cos\theta| < 0.984$ for the endcap region. The magnet return yoke consisting of barrel and endcap sections along with pole tips is instrumented for hadron calorimetry (HCAL) in the region $|\cos\theta| < 0.99$. Four layers of muon chambers cover the outside of the hadron calorimeter. Calorimeters close to the beam axis measure the luminosity using small angle Bhabha scattering events and complete the geometrical acceptance down to 24 mrad.

Monte Carlo simulation of the production and decay of $\tilde{t}_1(\tilde{b}_1)$ was performed as follows [12]. The $\tilde{t}_1\bar{\tilde{t}}_1(\tilde{b}_1\bar{\tilde{b}}_1)$ pairs were generated taking into account initial-state radiation [13]. The hadronisation process was subsequently performed to produce colourless $\tilde{t}_1$-hadrons ($\tilde{b}_1$-hadrons) and other fragmentation products according to the Lund string fragmentation scheme (JET-SET 7.4) [13, 14]. The parameters for perturbative QCD and fragmentation processes were optimised using the hadronic Z^0 decays measured by OPAL [15]. For the fragmentation of $\tilde{t}_1(\tilde{b}_1)$, the fragmentation function proposed by Peterson et $al.$ [13, 16] was used. The $\tilde{t}_1$-hadron ($\tilde{b}_1$-hadron) was formed from a $\tilde{t}_1$-quark ($\tilde{b}_1$-quark) and a spectator anti-quark or diquark. For the $\tilde{t}_1(\tilde{b}_1)$ decaying into $c\tilde{\chi}_1^0$ ($b\tilde{\chi}_1^0$), a colour string was stretched between the charm quark (the bottom quark) and the spectator. This colour singlet system was hadronised using the Lund scheme [13, 14]. Gluon bremsstrahlung was allowed in this process, and the Peterson function was also used for the charm quark and the bottom quark fragmentation. The signals for the decays $\tilde{t}_1 \to b\ell^+\tilde{\nu}$ were simulated in a similar manner.

One thousand events were generated at each point of a two dimensional grid of spacing of generally 5 GeV step in $(m_{\tilde{t}_1}, m_{\tilde{\chi}_1^0})$ for $\tilde{t}_1 \to c\tilde{\chi}_1^0$, in $(m_{\tilde{t}_1}, m_{\tilde{\nu}})$ for $\tilde{t}_1 \to b\ell^+\tilde{\nu}$ and $\tilde{t}_1 \to b\tau^+\tilde{\nu}$,

---

[3]A right-handed coordinate system is adopted, where the x-axis points to the centre of the LEP ring, and positive z is along the electron beam direction. The angles θ and ϕ are the polar and azimuthal angles, respectively.

and $(m_{\tilde{b}_1}, m_{\tilde{\chi}_1^0})$ for $\tilde{b}_1 \to b\tilde{\chi}_1^0$. Smaller steps were used for the case of small mass differences ($\Delta m = m_{\tilde{t}_1} - m_{\tilde{\chi}_1^0}$, $m_{\tilde{t}_1} - m_{\tilde{\nu}}$ or $m_{\tilde{b}_1} - m_{\tilde{\chi}_1^0}$). The mixing angles of the $\tilde{t}_1$ and $\tilde{b}_1$ were set to zero when these events were generated. The dependence of the detection efficiencies on these mixing angles is taken into account as a systematic error as described in Ref. [9].

The background processes were simulated as follows. The PYTHIA [13] generator was used to simulate multihadronic $(q\bar{q}(\gamma))$ events, and KORALZ [17] to generate $\tau^+\tau^-(\gamma)$ and $\mu^+\mu^-(\gamma)$ events. Bhabha events, $e^+e^- \to e^+e^-(\gamma)$, were generated with the BHWIDE program [18]. Two-photon processes are the most important background for the case of small mass differences, since in such cases signal events have small visible energy and small transverse momentum relative to the beam direction. Using the Monte Carlo generators PHOJET [19], PYTHIA [13] and HERWIG [20], hadronic events from two-photon processes were simulated in which the invariant mass of the photon-photon system $(M_{\gamma\gamma})$ was larger than 5.0 GeV. Monte Carlo samples for four-lepton events ($e^+e^-e^+e^-$, $e^+e^-\mu^+\mu^-$ and $e^+e^-\tau^+\tau^-$) were generated with the Vermaseren program [21]. The grc4f generator [22] was used for all four-fermion processes except for regions covered by the two-photon simulations. All interference effects of the various diagrams are taken into account in grc4f. Four-fermion processes in which at least one of the fermions is a neutrino constitute a serious background at large mass differences. The dominant contributions come from W^+W^-, γ^*Z^0 and $We\nu$ events. The Excalibur [23] and PYTHIA [13] generators were also used to study uncertainties in the grc4f generator. The generated signal and background events were processed through the full simulation of the OPAL detector [24], and the same analysis chain was applied as to the data.

3   Analysis

Since the event topologies of $\tilde{t}_1 \to c\tilde{\chi}_1^0$ and $\tilde{b}_1 \to b\tilde{\chi}_1^0$ are similar, the same selection criteria were used (Section 3.1, analysis A). In Section 3.2 (analysis B), the selection criteria for $\tilde{t}_1 \to b\ell^+\tilde{\nu}$ are discussed. These analyses are similar to those in Ref. [9], and the quality criteria therein were used to select good tracks and clusters. Variables used for the cuts, such as the total visible energy and the total transverse momentum, were calculated as follows. First, the four-momenta of the tracks and those of the EM and HCAL clusters not associated with charged tracks were summed. Whenever a calorimeter cluster had associated charged tracks, the expected energy deposited by the tracks was subtracted from the cluster energy to reduce double counting. If the energy of a cluster was smaller than the expected energy deposited by the associated tracks, the cluster energy was not used.

The following three preselections, which are common to analyses A and B, were applied: **(1)** The number of charged tracks was required to be at least four. The ratio of the number of good tracks to the total number of reconstructed tracks was required to be greater than 0.2 to reduce beam-gas and beam-wall background events. The visible mass of the event was also required to be larger than 3 GeV. **(2)** To reduce the background from two-photon processes, the energy deposited had to be less than 2 GeV in each silicon tungsten forward calorimeter, less than 2 GeV in each forward detector and less than 5 GeV in each side of the gamma-catcher detector. These detectors are located in the forward region ($|\cos\theta| > 0.98$) surrounding the beam pipe. **(3)** The visible energy in the region of $|\cos\theta| > 0.9$ was required to be less than 10% of the total visible energy. In addition, the polar angle of the missing momentum direction, θ_{miss}, was required to satisfy $|\cos\theta_{\mathrm{miss}}| < 0.9$ to reduce the two-photon and the $q\bar{q}(\gamma)$ background.

3.1 Analysis A: $\tilde{t}_1 \to c\tilde{\chi}_1^0$ and $\tilde{b}_1 \to b\tilde{\chi}_1^0$

The experimental signature for $\tilde{t}_1\bar{\tilde{t}}_1(\tilde{t}_1 \to c\tilde{\chi}_1^0)$ events and $\tilde{b}_1\bar{\tilde{b}}_1$ events is an acoplanar two-jet topology with a large transverse momentum with respect to the beam axis. The fragmentation functions of $\tilde{t}_1$ and $\tilde{b}_1$ are expected to be hard and the invariant mass of the charm (or bottom) quark and the spectator quark is small, therefore the jets are expected to be narrow.

The following five selections were applied: **(A1)** Events from two-photon processes were largely removed by demanding that the event transverse momentum with respect to the beam axis, P_t, be greater than 4.5 GeV. Since the hadron calorimeter, with its limited energy resolution, gives fluctuations in energy measurement, this selection was applied to P_t calculated both with and without the hadron calorimeter. Fig. 1(a) shows the distribution of P_t calculated with the hadron calorimeter after the preselections. **(A2)** The number of reconstructed jets was required to be exactly two. Jets were reconstructed using the Durham algorithm [25] with the jet resolution parameter of $y_{\text{cut}} = 0.005(E_{\text{vis}}/\sqrt{s})^{-1}$, where E_{vis} is the total visible energy. This E_{vis}-dependent y_{cut} parameter was necessary for good jet reconstruction over a wide range of $m_{\tilde{t}_1}$, $m_{\tilde{b}_1}$ and $m_{\tilde{\chi}_1^0}$. Furthermore, both reconstructed jets were required to contain at least two charged particles to reduce the $\tau^+\tau^-$ background where at least one of the τ's decayed into only one charged particle. **(A3)** The acoplanarity angle, ϕ_{acop}, is defined as π minus the azimuthal opening angle between the directions of the two reconstructed jets. To ensure the reliability of the calculation of ϕ_{acop}, both jet axes were required to have a polar angle satisfying $|\cos\theta_{\text{jet}}| < 0.95$. The value of ϕ_{acop} was required to be larger than 20°. **(A4)** 'Softness' was defined as $(\frac{M_1}{E_1} + \frac{M_2}{E_2})$, where M_1 and M_2 are the invariant masses of the two reconstructed jets, and E_1 and E_2 are the energies of the jets. The signal events have low values of 'Softness', whereas two-photon events which pass the acoplanarity cut have relatively large values as shown in Fig. 4 in Ref. [9]. It was required that $1.5 \times \text{Softness} < (P_t - 4.5)$, where P_t is calculated with the hadron calorimeter and given in units of GeV. **(A5)** The arithmetic mean of the invariant masses of the jets, $\bar{M}_{\text{jet}}$, was required to be smaller than 8 GeV. When the invariant mass of the event, M_{vis}, was larger than 65 GeV, a harder cut $\bar{M}_{\text{jet}} < 5$ GeV was applied to reduce background from W$e\nu$ events. Fig. 1(b) shows the $\bar{M}_{\text{jet}}$ distributions for data, the simulated background processes and typical $\tilde{t}_1\bar{\tilde{t}}_1$ events. As shown in this figure, jets from $\tilde{t}_1$ are expected to have low invariant masses.

The numbers of events remaining after each cut are listed in Table 1. The table also shows the corresponding numbers of simulated events for background processes and for two samples of simulated $\tilde{t}_1\bar{\tilde{t}}_1$ ($\tilde{t}_1 \to c\tilde{\chi}_1^0$) and one sample of $\tilde{b}_1\bar{\tilde{b}}_1$ events.

After all cuts, four events were observed in the data, which is consistent with the expected number of background events of 6.9±1.0, mainly from four-fermion processes.

The efficiencies for both $\tilde{t}_1\bar{\tilde{t}}_1$ and $\tilde{b}_1\bar{\tilde{b}}_1$ events are 30–60%, if the mass difference between $\tilde{t}_1(\tilde{b}_1)$ and $\tilde{\chi}_1^0$ is larger than 10 GeV. A modest efficiency of about 20% is obtained for a mass difference of 5 GeV for $\tilde{t}_1\bar{\tilde{t}}_1$ events. An additional efficiency loss of 3% (relative) arose from beam-related background in the silicon tungsten forward calorimeter, forward detector and gamma-catcher detectors, which was estimated using random beam crossing events. This inefficiency was taken into account in the limit calculation.

	data	total bkg.	$q\bar{q}(\gamma)$	$\ell^+\ell^-(\gamma)$	'$\gamma\gamma$'	4-f	$\tilde{t}_1\bar{\tilde{t}}_1$ and $\tilde{b}_1\bar{\tilde{b}}_1$		
$m_{\tilde{t}_1}$ (GeV) $m_{\tilde{b}_1}$ (GeV) $m_{\tilde{\chi}_1^0}$ (GeV)							90 – 85	90 – 70	– 90 70
cut (A1)	4073	4274	2157	497	121	1499	397	685	707
cut (A2)	995	1048	857	33.2	37.4	119	239	611	668
cut (A3)	75	83.7	0.18	0.25	7.7	75.6	237	564	609
cut (A4)	75	78.1	0.18	0.25	2.1	75.6	176	564	606
cut (A5)	4	6.9 (± 1.0)	0.00 ($^{+0.04}_{-0.00}$)	0.09 (± 0.04)	1.5 (± 0.9)	5.3 (± 0.4)	176	560	595

Table 1: Numbers of events remaining after each cut for various background processes are compared with data. The simulated background processes were normalised to the integrated luminosity of the data. The errors due to Monte Carlo statistics are also shown. Numbers for three simulated event samples of $\tilde{t}_1\bar{\tilde{t}}_1$ and $\tilde{b}_1\bar{\tilde{b}}_1$ are also given (each starting from 1000 events).

3.2 Analysis B: $\tilde{t}_1 \rightarrow b\ell\tilde{\nu}$

The experimental signature for $\tilde{t}_1\bar{\tilde{t}}_1(\tilde{t}_1 \rightarrow b\ell\tilde{\nu})$ events is two acoplanar jets plus two leptons with missing transverse momentum with respect to the beam axis. The momenta of the leptons and the missing transverse momentum depend strongly on the mass difference between $\tilde{t}_1$ and $\tilde{\nu}$. To obtain optimal performance, two sets of selection criteria (analyses B-L and B-H) were applied for small and large mass differences, respectively.

The numbers of events remaining after each cut are listed in Tables 2 and 3. The tables also show the corresponding numbers for the simulated background processes and for the simulated $\tilde{t}_1\bar{\tilde{t}}_1$ signals.

3.2.1 Small mass difference case

For the case of a small mass difference ($\Delta m \leq 10$ GeV), the following four selection criteria were applied: **(B-L1)** P_t was required to be greater than 5 GeV. **(B-L2)** The number of charged tracks was required to be at least six. Furthermore, the number of reconstructed jets was required to be at least four, since the signal would contain two hadronic jets plus two isolated leptons. Jets were reconstructed using the Durham algorithm [25] with the jet resolution parameter $y_{\text{cut}} = 0.004$. **(B-L3)** To examine the acoplanarity of the events remaining, jets were reconstructed using the Durham algorithm where the number of jets was forced to be two. To ensure a good measurement of the acoplanarity angle, $|\cos\theta_{\text{jet}}| < 0.95$ was required for both reconstructed jets. Finally, the acoplanarity angle, ϕ_{acop}, between these two jets was required to be greater than 15°. In the three-body decay, the transverse momentum carried by the $\tilde{\nu}$ with respect to the original $\tilde{t}_1$-momentum is smaller than that of $\tilde{\chi}_1^0$ in the two-body decay. When the $\tilde{t}_1$ is light, the outgoing $\tilde{\nu}$ is strongly boosted toward the direction of the parent $\tilde{t}_1$ and ϕ_{acop} for the signal becomes small. This is the reason why a looser acoplanarity angle cut was used. Fig. 1(c) shows the ϕ_{acop} distributions for the data, the simulated background processes and typical $\tilde{t}_1\bar{\tilde{t}}_1$ events. **(B-L4)** The total visible energy, E_{vis}, was required to be smaller than 60 GeV to reject four-fermion events.

	data	total bkg.	q$\bar{\text{q}}(\gamma)$	$\ell^+\ell^-(\gamma)$	'$\gamma\gamma$'	4-f	$\tilde{\text{t}}_1\bar{\tilde{\text{t}}}_1$	
$m_{\tilde{\text{t}}_1}$ (GeV)							75	90
$m_{\tilde{\nu}}$ (GeV)							68	80
cut (B-L1)	3900	4058	2030	480	88.7	1460	153	413
cut (B-L2)	1016	1023	307	0.11	6.4	709	132	373
cut (B-L3)	216	217	10.5	0.02	1.7	205	99	339
cut (B-L4)	0	2.1 (± 0.9)	0.04 (± 0.04)	0.00 ($^{+0.02}_{-0.00}$)	1.7 (± 0.9)	0.4 (± 0.1)	99	339

Table 2: Numbers of events remaining after each cut for various background processes are compared with data. The simulated background processes were normalised to the integrated luminosity of the data. The errors due to Monte Carlo statistics are also shown. Numbers for two simulated samples of $\tilde{\text{t}}_1\bar{\tilde{\text{t}}}_1$ are also given (each starting from 1000 events). In these samples, the branching fraction to each lepton flavour is assumed to be the same.

No events were observed in the data after all the cuts. This is consistent with the number of expected background events (2.1±0.9), mainly from two-photon background. The detection efficiencies are 30-35% if the mass difference between $\tilde{\text{t}}_1$ and $\tilde{\nu}$ is 10 GeV, and if the branching fraction to each lepton flavour is the same. Even if the branching fraction into b$\tau^+\tilde{\nu}_\tau$ is 100%, the efficiencies are 25-30%.

3.2.2 Large mass difference case

The selection criteria for a large mass difference ($\Delta m > 10$ GeV) were as follows: **(B-H1)** P_t was required to be greater than 6 GeV. **(B-H2)** The number of charged tracks was required to be at least six, and the number of reconstructed jets was required to be at least three. Jets were reconstructed with the same jet resolution parameter as in (B-L2). **(B-H3)** The same selection as (B-L3) was applied on the ϕ_{acop} variable to reject q$\bar{\text{q}}(\gamma)$ events. **(B-H4)** A candidate event was required to contain at least one lepton, since a signal event would contain two isolated leptons. The selection criteria for leptons are given in Ref. [9]. **(B-H5)** The invariant mass of the event excluding the most energetic lepton, M_{hadron}, was required to be smaller than 60 GeV in order to reject W$^+$W$^- \to \nu\ell$q$\bar{\text{q}}'$ events. As shown in Fig. 1(d), a large fraction of four-fermion events was rejected using this requirement. Furthermore the invariant mass excluding all identified leptons was required to be smaller than 40 GeV. **(B-H6)** Finally, the visible mass of event, M_{vis}, must be smaller than 80 GeV to reduce W$^+$W$^-$ background events in which one of W decays into $\tau\nu$ and the other into q$\bar{\text{q}}'$(g). If one jet from q$\bar{\text{q}}'$(g) was misidentified as a tau lepton, this event could pass the previous cut (B-H5).

Three events were observed in the data, which is consistent with the number of expected background events (1.9 $^{+0.5}_{-0.3}$). The dominant background arises from four-fermion processes. The detection efficiencies are 25-60%, if the mass difference between the $\tilde{\text{t}}_1$ and $\tilde{\nu}$ is 10 GeV, and if the $\tilde{\nu}$ is heavier than 30 GeV. The detection efficiencies for $\tilde{\text{t}}_1 \to $ b$\tau^+\tilde{\nu}_\tau$ were found to be slightly smaller than in the case where the branching fraction to each lepton flavour is assumed to be the same.

	data	total bkg.	$q\bar{q}(\gamma)$	$\ell^+\ell^-(\gamma)$	'$\gamma\gamma$'	4-f	$\tilde{t}_1\bar{\tilde{t}}_1$		
$m_{\tilde{t}_1}$ (GeV)							90	90	90
$m_{\tilde{\nu}}$ (GeV)							80	70	45
cut (B-H1)	3576	3683	1802	448	53.2	1380	299	608	657
cut (B-H2)	2261	2399	1125	3.38	10.5	1261	299	605	647
cut (B-H3)	618	638	37.5	0.65	0.85	599	280	570	569
cut (B-H4)	444	478	15.5	0.53	0.00	462	239	534	541
cut (B-H5)	5	4.3	0.10	0.09	0.00	4.1	239	534	447
cut (B-H6)	3	1.9 $\left(\begin{smallmatrix}+0.5\\-0.3\end{smallmatrix}\right)$	0.10 (± 0.03)	0.04 (± 0.03)	0.00 $\left(\begin{smallmatrix}+0.5\\-0.00\end{smallmatrix}\right)$	1.8 (± 0.3)	239	534	437

Table 3: Numbers of events remaining after each cut for various background processes are compared with data. The simulated background processes were normalised to the integrated luminosity of the data. The errors due to Monte Carlo statistics are also shown. Numbers for three simulated samples of $\tilde{t}_1\bar{\tilde{t}}_1$ are also given (each starting from 1000 events). In these samples, the branching fraction to each lepton flavour is assumed to be the same.

4 Results

The observed number of candidate events in each case is consistent with the expected number of background events. Since no evidence for $\tilde{t}_1\bar{\tilde{t}}_1$ and $\tilde{b}_1\bar{\tilde{b}}_1$ pair-production has been observed, lower limits on $m_{\tilde{t}_1}$ and $m_{\tilde{b}_1}$ are calculated.

The systematic errors on the expected number of signal and background events were estimated in the same manner as in the previous paper [9]. The main sources of systematic errors on signal are uncertainties in the $\tilde{t}_1$ and $\tilde{b}_1$ fragmentation (5–10%) and in Fermi motion of the spectator quark (3–8%). The main sources of systematic errors on background are uncertainties in the generator of four-fermion processes (20%) and statistical fluctuation in two-photon Monte Carlo samples. Detailed descriptions are given in Ref. [9]. Systematic errors are taken into account when calculating limits [26].

Figure 2 shows the 95% C.L. excluded regions in the $(m_{\tilde{t}_1}, m_{\tilde{\chi}_1^0})$ plane for $\tilde{t}_1 \rightarrow c\tilde{\chi}_1^0$. In this figure there is a triangular region of $m_{\tilde{t}_1} - m_{\tilde{\chi}_1^0} > m_{W^\pm} + m_b$, in which $\tilde{t}_1 \rightarrow b\tilde{\chi}_1^0 W^+$(on shell) through a virtual chargino becomes dominant even if the chargino is heavy. This region is not excluded. Since the momenta of b and $\tilde{\chi}_1^0$ are small at the current centre-of-mass energy, the signal topology is very similar to W^+W^- background events.

Figures 3(a) and (b) show the 95% C.L. excluded regions in the $(m_{\tilde{t}_1}, m_{\tilde{\nu}})$ plane for $\tilde{t}_1 \rightarrow b\ell\tilde{\nu}$ (ℓ= e,μ,τ) and $\tilde{t}_1 \rightarrow b\tau^+\tilde{\nu}_\tau$, respectively. The branching fraction to each lepton flavour ℓ^+ depends on the composition of the lightest chargino [4]. As the chargino becomes Higgsino-like, the branching fraction into $b\tau^+\tilde{\nu}_\tau$ becomes large. In the limit that the chargino is a pure Wino state, the branching fraction to each lepton flavour is the same. Two extreme cases in which the branching fraction to each lepton flavour is the same, or the branching fraction into $b\tau^+\tilde{\nu}_\tau$ is 100%, were considered here.

The 95% C.L. mass bounds of $\tilde{t}_1$ are listed in Table 4 for various values of $\theta_{\tilde{t}}$. Assuming that $\tilde{t}_1$ decays into $c\tilde{\chi}_1^0$, and the mass difference between $\tilde{t}_1$ and $\tilde{\chi}_1^0$ is greater than 10 GeV, $\tilde{t}_1$ is found to be heavier than 90.3 GeV for $\theta_{\tilde{t}} = 0.0$. A lower limit of 87.2 GeV is obtained even if

$\tilde{t}_1$ decouples from the Z^0 boson ($\theta_{\tilde{t}}$=0.98 rad). When $\tilde{t}_1$ decays into $b\ell\nu$, the lower limit on $m_{\tilde{t}_1}$ is 90.5 GeV for the zero mixing angle case, assuming that the mass difference between $\tilde{t}_1$ and $\tilde{\nu}$ is greater than 10 GeV and that the branching fraction to each lepton flavour is the same. These limits improve significantly (about 10 GeV) the previous OPAL limits [9].

Lower limit on $m_{\tilde{t}_1}$ (GeV)				
	$\tilde{t}_1 \to c\tilde{\chi}_1^0$		$\tilde{t}_1 \to b\ell\tilde{\nu}$ $\ell = e, \mu, \tau$	$\tilde{t}_1 \to b\tau\tilde{\nu}_\tau$ Br = 100%
$\theta_{\tilde{t}}$ (rad)	$\Delta m \geq 5$ GeV	$\Delta m \geq 10$ GeV	$\Delta m \geq 10$ GeV	$\Delta m \geq 10$ GeV
0.0	89.1	90.3	90.5	90.0
$\leq \frac{1}{8}\pi$	88.6	89.9	89.9	89.5
$\leq \frac{1}{4}\pi$	86.8	87.7	88.6	87.9
0.98	86.4	87.2	88.0	87.5

Table 4: The excluded $m_{\tilde{t}_1}$ region at 95% C.L. ($\Delta m = m_{\tilde{t}_1} - m_{\tilde{\chi}_1^0}$ or $m_{\tilde{t}_1} - m_{\tilde{\nu}}$).

The 95% C.L. excluded regions in the ($m_{\tilde{b}_1}$, $m_{\tilde{\chi}_1^0}$) plane are shown in Fig. 4 for two cases $\theta_{\tilde{b}}$= 0 and 1.17 rad. The numerical mass bounds are listed in Table 5 for various $\theta_{\tilde{b}}$. These bounds are significantly stronger than the previous OPAL limits [9] by about 10 GeV. The lower limit on the $\tilde{b}_1$-mass is found to be 88.6 GeV, if Δm is greater than 7 GeV and $\theta_{\tilde{b}} = 0.0$. When Δm is greater than 10 GeV and $\tilde{\chi}_1^0$ is heavier than 30 GeV, $\tilde{b}_1$ is found to be heavier than 89.8 GeV. If the $\tilde{b}_1$ decouples from the Z^0 boson ($\theta_{\tilde{b}}$=1.17 rad), the lower limit is 74.9 GeV. Since the electromagnetic charge of $\tilde{b}_1$ is half that of $\tilde{t}_1$, the coupling between γ and $\tilde{b}_1$ is weaker than between γ and $\tilde{t}_1$. Therefore the production cross-section of $\tilde{b}_1\bar{\tilde{b}}_1$ is strongly suppressed when the $\tilde{b}_1$ decouples from the Z^0 boson.

Lower limit on $m_{\tilde{b}_1}$ (GeV) ($\tilde{b}_1 \to b\tilde{\chi}_1^0$)		
$\theta_{\tilde{b}}$ (rad)	$\Delta m \geq 7$ GeV	$\Delta m \geq 10$ GeV $m_{\tilde{\chi}_1^0} \geq 30$ GeV
0.0	88.6	89.8
$\leq \frac{1}{8}\pi$	87.8	89.2
$\leq \frac{1}{4}\pi$	82.2	85.0
1.17	65.8	74.9

Table 5: The excluded $m_{\tilde{b}_1}$ region at 95% C.L. ($\Delta m = m_{\tilde{b}_1} - m_{\tilde{\chi}_1^0}$)

5 Summary and Conclusion

A data sample of 182.1 pb^{-1} collected using the OPAL detector at $\sqrt{s}$ =188.6 GeV has been analysed to search for pair production of the scalar top quark and the scalar bottom quark predicted by supersymmetric theories assuming R-parity conservation. No evidence was found above the background level expected from the Standard Model.

The 95% C.L. lower limit on the scalar top quark mass is 90.3 GeV, if the mixing angle of the scalar top quark is zero. If the $\tilde{t}_1$ decouples from the Z^0 boson, a lower limit of 87.2 GeV is

obtained. These limits were estimated assuming that the scalar top quark decays into a charm quark and the lightest neutralino and that the mass difference between the scalar top and the lightest neutralino is larger than 10 GeV.

Assuming a relatively light scalar neutrino ($m_{\tilde{\nu}} \leq m_{\tilde{t}_1} - m_b$), the complementary decay mode, in which the scalar top quark decays into a bottom quark, a charged lepton and a scalar neutrino, has also been studied. If the mass difference between the scalar top quark and the scalar neutrino is greater than 10 GeV and if the mixing angle of the scalar top quark is zero, the 95% C.L. lower limit on the scalar top quark mass is 90.5 GeV. This limit is obtained assuming that the branching fraction to each lepton flavour is the same. If the branching fraction to the tau lepton is 100%, a lower limit of 90.0 GeV is obtained.

The 95% C.L. mass limit on the light scalar bottom quark is found to be 88.6 GeV, assuming that the mass difference between the scalar bottom quark and the lightest neutralino is greater than 7 GeV and that the mixing angle of the scalar bottom quark is zero. If the mass difference is greater than 10 GeV and the lightest neutralino is heavier than 30 GeV, the mass limit on the light scalar bottom quark is 89.8 GeV for zero mixing angle. If the scalar bottom quark decouples from the Z^0 boson, a lower limit of 74.9 GeV is obtained.

Acknowledgements

References

[1] M. Drees and K. Hikasa, Phys. Lett. **B252** (1990) 127;
K. Hikasa and M. Kobayashi, Phys. Rev. **D36** (1987) 724.

[2] A. Bartl, W. Majerotto and W. Porod, Z. Phys. **C64** (1994) 499.

[3] P. Fayet, Phys. Lett. **B69** (1977) 489.

[4] OPAL Collab., K. Ackerstaff *et al.*, Z. Phys. **C75** (1997) 409.

[5] D0 Collab., F. Abachi *et al.*, Phys. Rev. Lett. **76** (1996) 2222.

[6] OPAL Collab., R. Akers *et al.*, Phys. Lett. **B337** (1994) 207.

[7] OPAL Collab., K. Ackerstaff *et al.*, Phys. Lett. **B389** (1996) 197.

[8] ALEPH Collab., R. Barate *et al.*, Phys. Lett. **B413** (1997) 431;
DELPHI Collab., P. Abreu *et al.*, Eur. Phys. J. **C6** (1999) 385.

[9] OPAL Collab., K. Ackerstaff *et al.*, Eur. Phys. J. **C6** (1999) 225.

[10] ALEPH Collab., R. Barate *et al.*, Phys. Lett. **B434** (1998) 189;
L3 Collab., M. Acciarri *et al.*, Phys. Lett. **B445** (1999) 428.

[11] OPAL Collab., K. Ahmet *et al.*, Nucl. Instr. Meth. **A305** (1991) 275;
S. Anderson *et al.*, Nucl. Instr. Meth. **A403** (1998) 326;
B.E. Anderson *et al.*, IEEE Trans. Nucl. Sci. **41** (1994) 845.

[12] E. Accomando *et al.*, in 'Physics at LEP2', eds. G. Altarelli, T. Sjöstrand and F. Zwirner, CERN 96-01, vol. 2, 299.

[13] T. Sjöstrand, Comp. Phys. Comm. **82** (1994) 74.

[14] B. Andersson *et al.*, Phys. Rep. **97** (1983) 31.

[15] OPAL Collab., G. Alexander *et al.*, Z. Phys. **C69** (1996) 543.

[16] C. Peterson, D. Schlatter, I. Schmitt and P.M. Zerwas, Phys. Rev. **D27** (1983) 105.

[17] S. Jadach, B.F.L. Ward and Z. Wąs, Comp. Phys. Comm. **79** (1994) 503.

[18] S. Jadach, W. Płaczek, and B.F.L. Ward, in 'Physics at LEP2', eds. G. Altarelli, T. Sjöstrand and F. Zwirner, CERN 96-01, vol. 2, 286.

[19] R. Engel and J. Ranft, Phys. Rev. **D54** (1996) 4244.

[20] G. Marchesini *et al.*, Comp. Phys. Comm. **67** (1992) 465.

[21] J.A.M. Vermaseren, Nucl. Phys. **B229** (1983) 347.

[22] J. Fujimoto *et al.*, Comp. Phys. Comm. **100** (1997) 128.

[23] F.A. Berends, R. Pittau, R. Kleiss, Comp. Phys. Comm. **85** (1995) 437.

[24] J. Allison *et al.*, Nucl. Instr. Meth. **A317** (1992) 47.

[25] S. Catani *et al.*, Phys. Lett. **B269** (1991) 432.

[26] R.D. Cousins and V.L. Highland, Nucl. Instr. Meth. **A320** (1992) 331.

[27] ALEPH Collab., D. Decamp *et al.*, Phys. Rep. **216** (1992) 253;
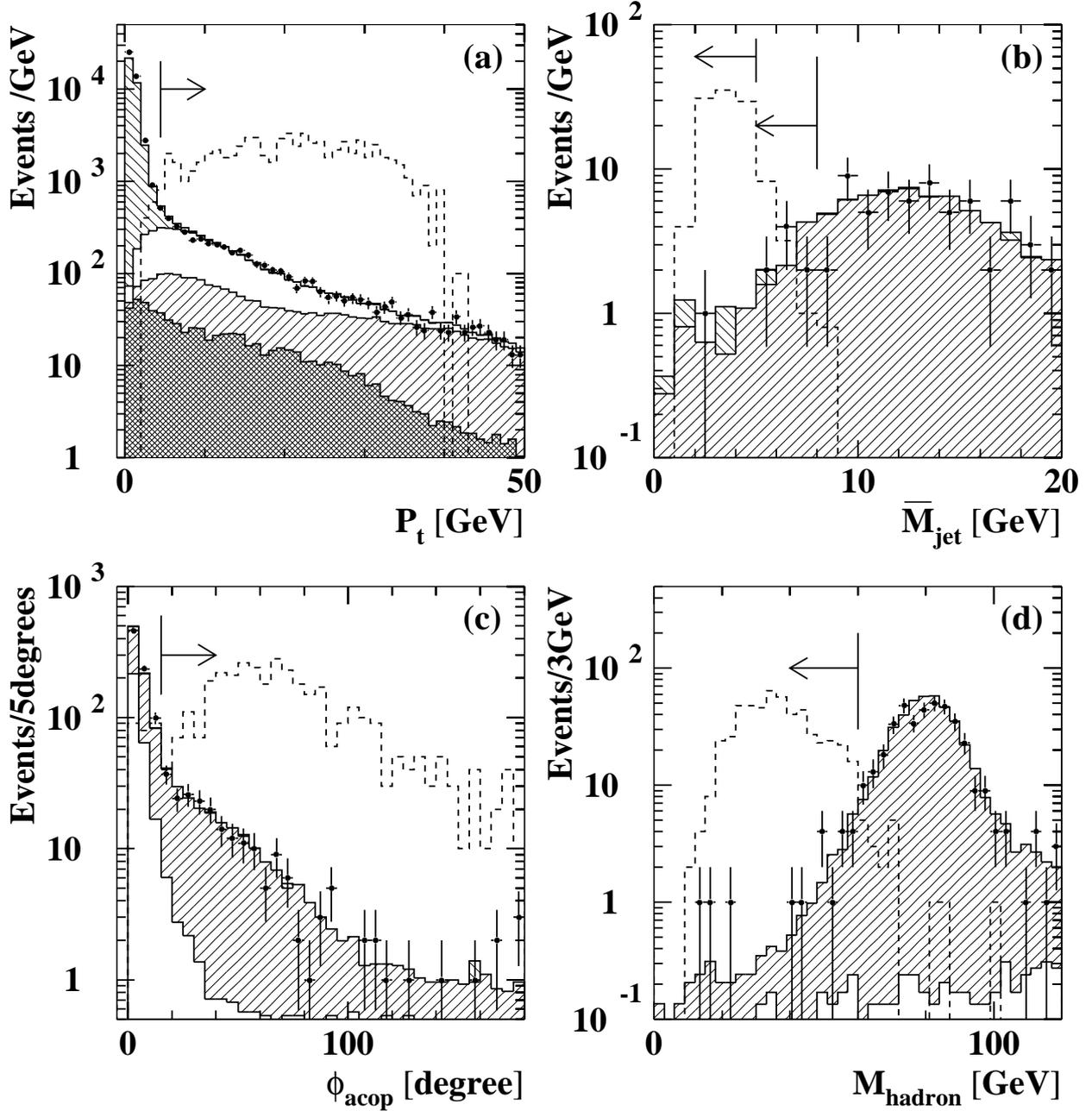L3 Collab., O. Adriani *et al.*, Phys. Rep. **236** (1993) 1.

OPAL

Figure 1: Distributions of (a) P_t before cut (A1), (b) $\bar{M}_{\mathrm{jet}}$ before cut (A5), (c) ϕ_{acop} before cut (B-L3), (d) invariant mass excluding the most energetic lepton before cut (B-H5), for the data, simulated background events and typical $\tilde{t}_1\bar{\tilde{t}}_1$ predictions. In these figures, the distribution of the data is shown as points with error bars. The background processes are as follows: dilepton events (cross-hatched area), two-photon processes (negative slope hatched area), four-fermion processes (positive slope hatched area), and multihadronic events (open area). The arrows show the cut positions. In (b), the left (right) arrow indicates the cut position for $M_{\mathrm{vis}} > 65$ GeV ($M_{\mathrm{vis}} < 65$ GeV). The predictions for $\tilde{t}_1\bar{\tilde{t}}_1$ signals are shown by the dashed lines. The $\tilde{t}_1\bar{\tilde{t}}_1$ predictions show the cases of $(m_{\tilde{t}_1}, m_{\tilde{\chi}_1^0})=(90$ GeV, 70 GeV$)$ in (a) and (b), $(m_{\tilde{t}_1}, m_{\tilde{\nu}})=(90$ GeV, 80 GeV$)$ in (c), and $(m_{\tilde{t}_1}, m_{\tilde{\nu}})=(90$ GeV, 45 GeV$)$ in (d). The normalisations of the $\tilde{t}_1\bar{\tilde{t}}_1$ predictions are arbitrary.
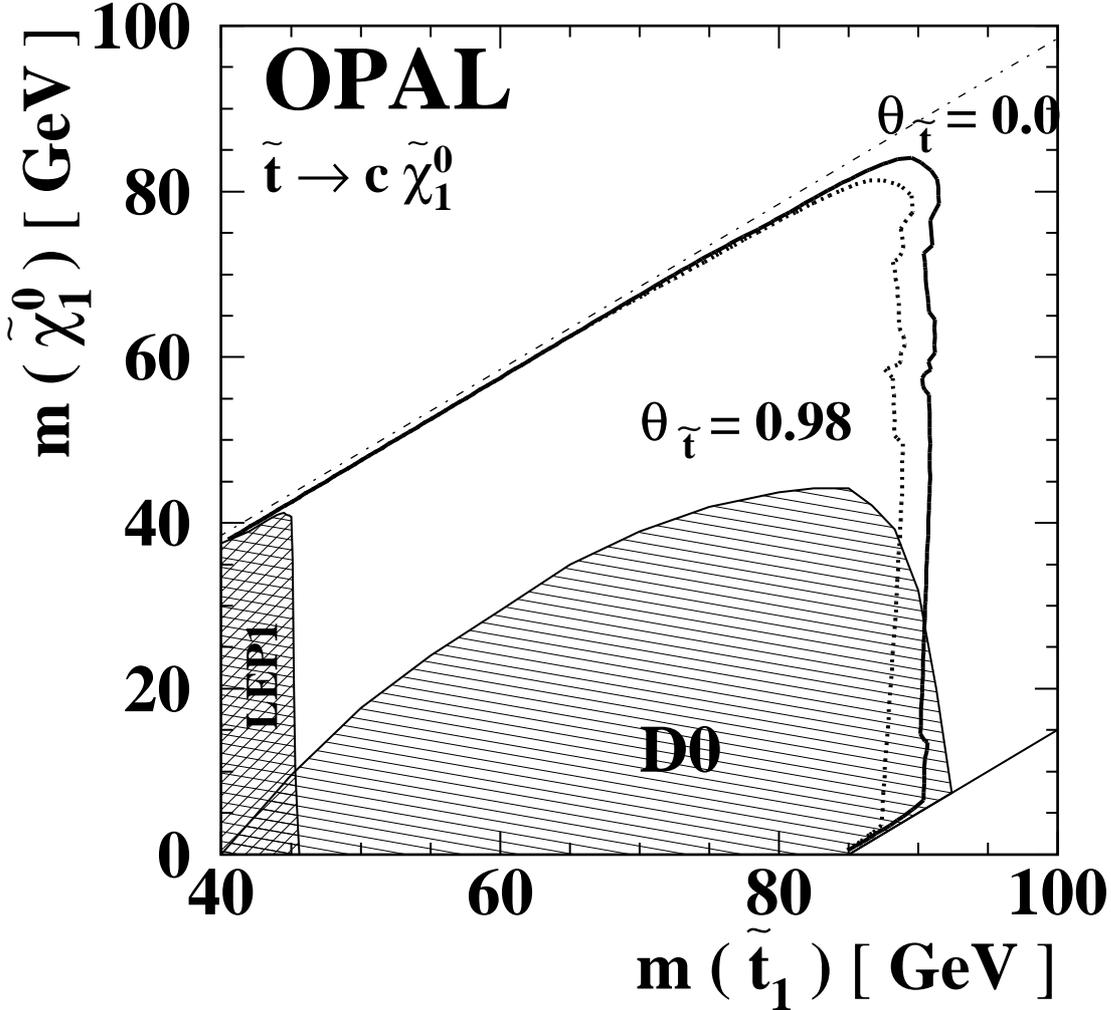
14

Figure 2: The 95% C.L. excluded regions in the $(m_{\tilde{t}_1}, m_{\tilde{\chi}_1^0})$ plane assuming that $\tilde{t}_1$ decays into $c\tilde{\chi}_1^0$. The solid line shows the limit for zero mixing angle of $\tilde{t}_1$, and the dotted line shows the limit for a mixing angle of 0.98 rad ($\tilde{t}_1$ decouples from the Z^0 boson). The cross-hatched region has already been excluded by OPAL searches at LEP1 [6]. The singly-hatched region is excluded by the D0 Collaboration [5]. The dash-dotted straight line shows the kinematic limit for the $\tilde{t}_1 \rightarrow c\tilde{\chi}_1^0$ decay. In the triangular region of $m_{\tilde{t}_1} - m_{\tilde{\chi}_1^0} > m_{W^\pm} + m_b$, the decay $\tilde{t}_1 \rightarrow b\tilde{\chi}_1^0 W^+$(on shell) through a virtual chargino becomes dominant. This region is not excluded.
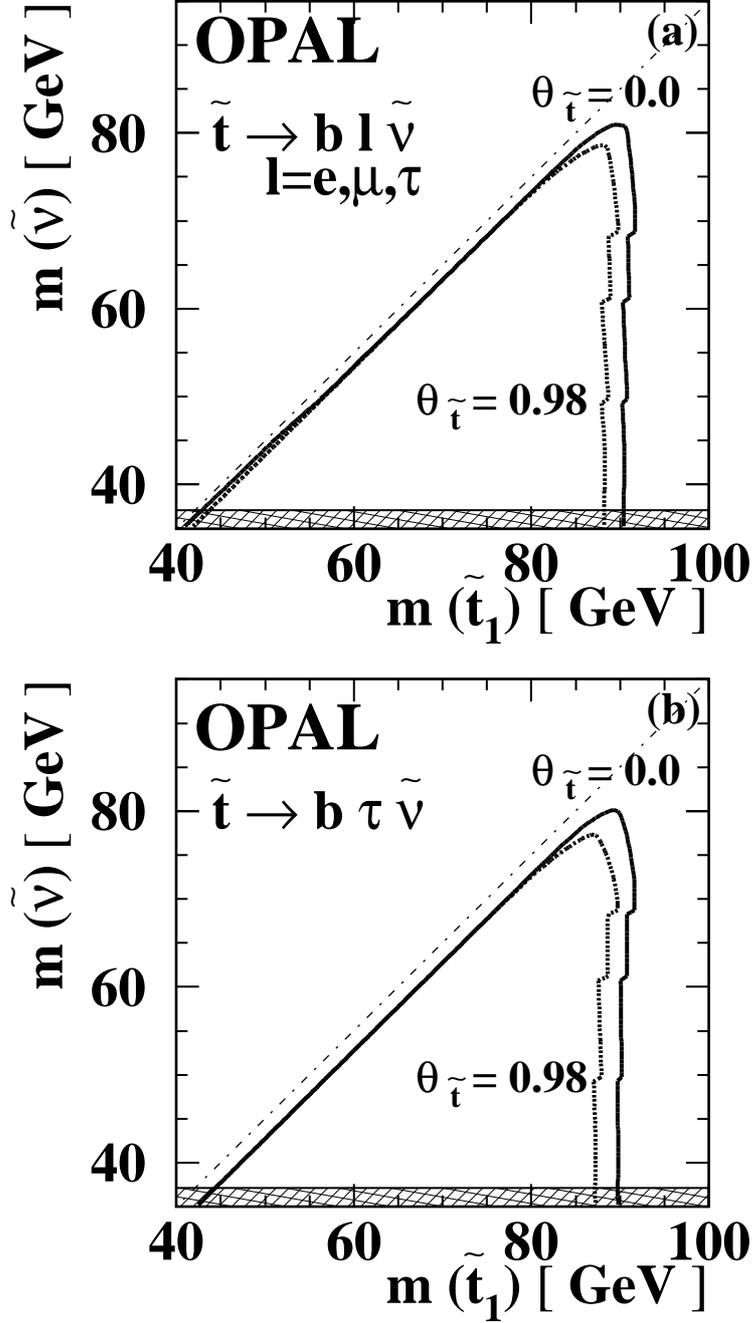
15

Figure 3: The 95% C.L. excluded regions in the $(m_{\tilde{t}_1}, m_{\tilde{\nu}})$ plane assuming that the $\tilde{t}_1$ decays into $b\ell\tilde{\nu}$; (a) the branching fraction to each lepton flavour is the same; (b) $\tilde{t}_1$ always decays into $b\tau\tilde{\nu}_\tau$. The solid lines show the limits where the mixing angle of $\tilde{t}_1$ is assumed to be 0.0 rad, and the dotted lines show the limits for a mixing angle of 0.98 rad (decoupling case). The hatched region has been excluded at LEP1 [27], and the dash-dotted diagonal line shows the kinematic limit for the $\tilde{t}_1 \to b\ell\tilde{\nu}$ decay.
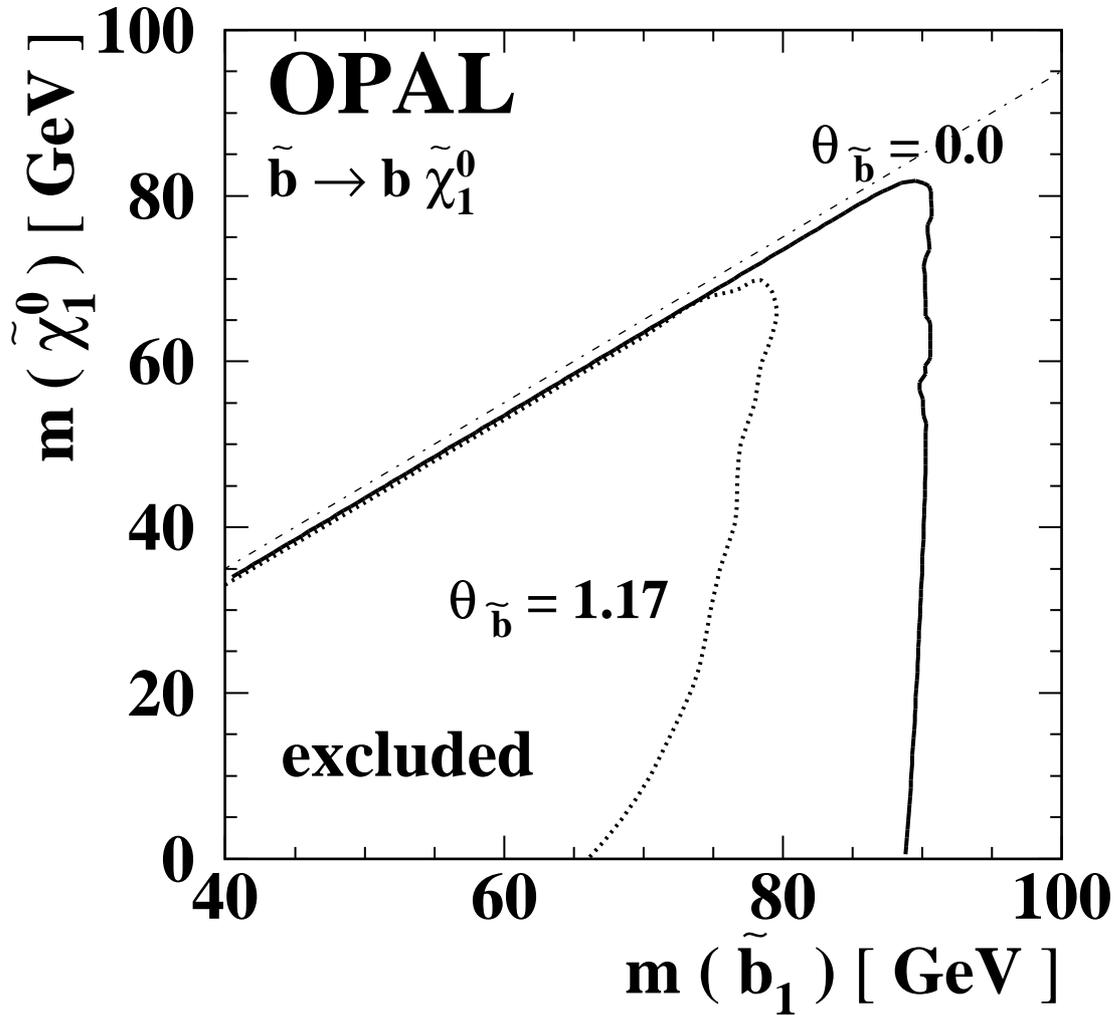
Figure 4: The 95% C.L. excluded regions in the $(m_{\tilde{b}_1}, m_{\tilde{\chi}_1^0})$ plane, assuming that $\tilde{b}_1$ decays into $b\tilde{\chi}_1^0$. The solid line shows the limit where the mixing angle of $\tilde{b}_1$ is assumed to be 0.0 rad, and the dotted line shows the limits for a mixing angle of 1.17 rad ($\tilde{b}_1$ decouples from the Z^0 boson).